

SURFACE CHARACTERIZATION OF PLASMA SPRAYED HYDROXYAPATITE COATINGS

Limin Sun, Christopher C. Berndt, A. **Kucuk** and R S. Lima
Department of Materials Science and Engineering
State University of New **York** at Stony Brook
Stony Brook, New York, 11794-2275 USA

K.A. Khor
School of Mechanical and Production Engineering
Nanyang Technological University, Singapore 639798

ABSTRACT

Plasma sprayed hydroxyapatite (HA) coatings have been widely used for dental and orthopedic applications for fast fixation between the implant and the human anatomy. In this study, the HA coatings were atmospherically plasma sprayed (**APS**) using different spray power and **stand-off** distance (SOD), and the coating surfaces were characterized using various methods. X-ray **diffraction** (XRD) revealed the presence of crystalline HA, amorphous calcium phosphate (ACP) and some other crystalline phases including **tricalcium** phosphate (α -TCP and β -TCP), **tetracalcium** phosphate (TTCP) and calcium oxide (CaO). Fourier transform **infrared** (FTIR) spectroscopy showed that both OH and PO_4^{3-} bands of HA changed after spraying and the HA phase identified by XRD **was** actually the solid solution of oxyapatite (**OAp**) in HA, **i.e.**, oxyhydroxyapatite (OHA). The phase composition of the HA coatings varied with respect to the spray power and SOD. The Surface morphology and roughness were analyzed via scanning electron microscopy (SEM) and **profilometry** respectively, and the results related to the phase composition

INTRODUCTION

Plasma sprayed hydroxyapatite [$\text{Ca}_{10}(\text{PO}_4)_6(\text{OH})_2$, **i.e.**, HA] coatings on metallic implants have attracted great interest in the biomedical field due to the good strength and ductility of the metal and the increased **biocompatibility** of the HA as well as the fast cementless **fixation**.^{1,2} HA coating also enhances the bone **ingrowth**³ and protects the surrounding bone **against** metal-ion release **from** the metallic implant.⁴ It has been indicated that the composition and the **structure** of the plasma sprayed HA coating are different from those of the original HA feedstock due to the high plasma temperature and rapid cooling **rate**.² Some amorphous calcium phosphate (ACP), **tricalcium** phosphate (α -TCP and β -TCP), **tetracalcium** phosphate (TTCP) and calcium oxide (CaO) were detected using X-ray diffraction (XRD) in previous **studies**.^{1,5,6,7} In addition, a solid solution of oxyapatite (**OAp**) in HA, **i.e.**, oxyhydroxyapatite (OHA), also formed in HA coatings due to the **dehydroxylation** of HA, which was usually examined using Fourier Transform Infrared (**FTIR**) **spectroscopy**.^{6,8,9} Hydroxyapatite is a very stable phase in body fluids, but the dissolution rates of all new phases were found much higher than HA, which is in the order of $\text{ACP} \gg \text{TTCP} > \alpha\text{-TCP} > \text{OHA} > \beta\text{-TCP} \gg \text{HA}$ and will possibly lead to **degradation** of the HA **coating**.^{8,10} Calcium oxide has no biocompatibility and dissolves **significantly** faster than TCP¹¹ and, thus, it

is a detrimental phase for **the** overall implant **structure**. The phase composition of HA coatings generally varied as a result of different spray parameters and led to different dissolution rates of HA coatings in physiological solutions. The coating surface is especially of importance, since, once implanted, it is directly in contact with the bone and body fluid, and the dissolution rate of the surface will be a deciding factor for both the fixation period and the fixation strength between the coating **and bone**.¹² In addition to the phase composition of the coating surface, some **microstructural** evolution characteristics such as surface morphology and surface roughness also **affect** the dissolution rate of the HA coating.

The present work aims to investigate the surface characteristics of the HA coatings sprayed using different spray power and SOD. These technological details of thermal spray are expected to manifest themselves with regards to the *in vitro* and *in vivo* behavior of the HA coatings.

EXPERIMENTAL

Plasma Spraying

The feedstock were fully crystalline pure HA powders with a particle size distribution in the range of 10 – 120 μm . They were produced by spray drying followed by heat treatment. A Metco 3MB plasma torch with a GH nozzle (**Sulzer Metco**, Westbury, NY) was used for the atmospheric plasma spray (APS) process. Argon was used as the **primary gas** (at 50 slpm) and the carrier gas (at 3.65 slpm). Hydrogen was used as the **secondary gas** while its volume was adjusted to obtain different spray voltages. The powders were sprayed at 14 g/min and three types of spray power and two stand-off distances were used. The mild steel substrates were grit-blasted using Al_2O_3 grit and cleaned with acetone before spraying. All coatings were sprayed for the **same** number of passes and the thickness varied **from** 70 to 120 μm owing to **the** different deposition efficiencies.

Surface Characterization

The HA coating surfaces were scanned using a computer controlled **Philips PW 1729 X-ray diffractometer** with $\text{CuK}\alpha_1$ radiation at 40 kV and 30 mA. **The goniometer was** set at a scan rate of 0.005 %/sec over a 2θ range of **20-60°**. The acquired X-ray diffraction (XRD) pattern were identified by comparing with the JCPDS (Joint Committee on Powder **Diffraction Standard**) standards.³ The crystallinity of the HA coating was calculated using the following equation:^{1,14}

$$\text{Crystallinity (\%)} = \frac{A_c}{A_c + A_A} \times 100\% \quad (1)$$

Where A_c is the total integrated intensity of all HA peaks within **25-37° (ALL** angular terms are expressed in terms of 2θ). It is calculated by multiplying **the** area of the most intensive (211) peak of HA by 3.23, which is the ratio of the total intensity of all HA peaks within **25-37°** in JCPDS card (9-432) to the intensity of the (211) **peak**. The term "**A_A**" is the integrated intensity of the ACP phase, which **was** evaluated using the area of the amorphous hump between **25° and 37°**. **ALL** peak area calculations were performed using curve fitting and the **error** was estimated within five percent of the mean value.

A Nicolet **MAGNA-IR 760** spectrometer was **used** to record the **infrared** spectra of the HA powders and coatings. Feedstock powders or powders **scraped from the** coating surface were mixed with **KBr** at a weight ratio of around **1:20** and pressed into pellets. The spectra were **acquired over** the range of **400 - 4000 cm^{-1}** with a resolution of **4 cm^{-1}** . Each spectrum was scanned 4 times to **increase the** signal-to-noise ratio.

The HA coating surfaces were coated with a thin layer of carbon and then examined using a **Philips ISI-SX-30 SEM** to ascertain the morphology. The surface roughness (R_a) of the HA

coating was measured using a Hommel Tester T1000 Profilometer and each coating was measured 15 times to obtain average value.

RESULTS AND DISCUSSION

Phase Analysis

XRD analysis: Figure 1 shows the XRD patterns of the HA coatings sprayed at different powers and SODs. At the same SOD, when the spray power increased, the overall intensity of HA peaks decreased and the amorphous hump became more obvious. Meanwhile, the peaks of all impurity phases (α -TCP, β -TCP, TTCP and CaO) also increased. On the other hand, at the same spray power, the intensity of all HA peaks decreased appreciably and the amorphous hump became significant when the SOD increased from 80 mm to 160 mm. The peaks of α -TCP, β -TCP and TTCP did not exhibit obvious changes while the CaO peaks increased significantly with the SOD at higher spray power.

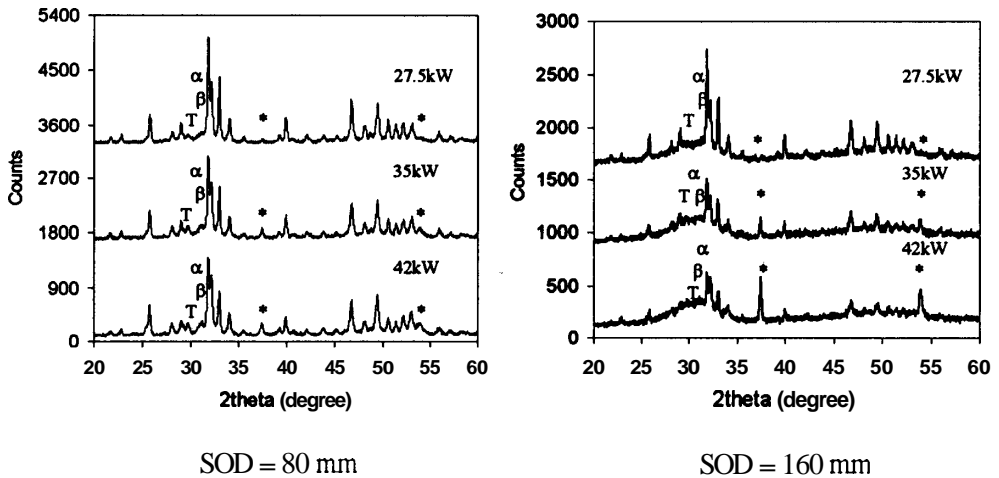


Figure 1. XRD patterns of HA coatings sprayed at different spray power and SOD. “ α ” is α -TCP, “ β ” is β -TCP, “T” is TTCP, “*” is CaO. All other peaks belong to HA.

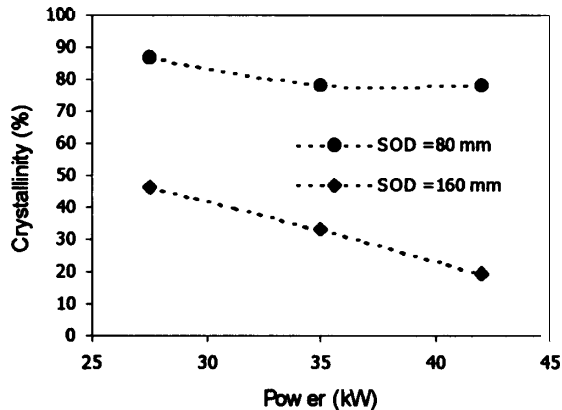


Figure 2. Crystallinity of HA coatings sprayed at different power and SOD

The crystallinity of the HA coatings is shown in Fig. 2. The crystallinity decreased with the increase of the spray power and decreased significantly when the SOD increased from 80 mm to 160 mm. This behavior occurs because an increase in power **causes** a higher plasma temperature and, therefore, more powders will be likely to melt, **thus**, more ACP formed from the melt **as** the result of the rapid cooling rate of the plasma spray process. In addition, the cooling rate and the dehydroxylation also became higher, which also promoted the **formation** of ACP. On the other hand, as the SOD increased, the substrate temperature decreased and the cooling rate greatly increased. As well, the HA powders **suffered** more melting and dehydroxylation, thus, more ACP formed. Another **important** reason for the crystallinity decrease at longer SOD is that some of the **unmelted** larger particles were blown away before they impacted on the substrate. This phenomenon is evidenced by the fact that the deposition efficiency (measured by the coating thickness) decreased around **40%** when the SOD increased from 80 mm to 160 mm.

The quantitative analysis of impurity phases and their formation mechanism have been shown in another **work**.⁷ Worthy of stress here is the change of **CaO** content for different coatings, which was found to affect the characteristics of the OH band in the **FTIR** spectra of the HA coatings.

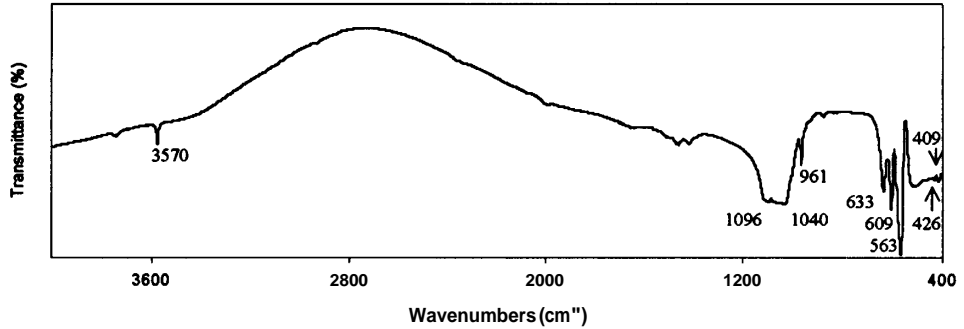
FTIR analysis: In addition to XRD, FTIR is another important characterization method for plasma sprayed HA coatings since it can give more features which can not be easily obtained using XRD. The **spectra** of HA powders and coatings were shown in Fig. 3. The **961 cm⁻¹** band, characteristic of **non-degenerate** symmetric stretching of the **PO₄** group (**v₁**) in HA, disappeared in all HA coatings. The doubly degenerate **O-P-O** bending band (**v₂**) at **434 cm⁻¹** and **471 cm⁻¹** in **references**^{15,16} were not visible in the spectra of both HA powders and coatings, but there were two weak **peaks** at **409 cm⁻¹** and **426 cm⁻¹** in the **spectra** of HA powders. The original asymmetric **O-P-O** stretching vibration band (**v₃**) at **1040 cm⁻¹** and **10% cm⁻¹** still existed in HA coatings, while the splitting of these two bands decreased with the crystallinity of the HA coatings. The triply degenerate asymmetric **O-P-O** bending band (**v₄**) at **609 cm⁻¹** and **563 cm⁻¹** (sometimes along with a weaker shoulder at **549 cm⁻¹**) also still existed and their **splitting** exhibited the same trend with respect to the crystallinity of the HA coatings.

In addition to **PO₄³⁻** groups, both of the two characteristic OH bands of HA changed greatly after spraying. The flexural band at **633 cm⁻¹** disappeared in the spectra of all coatings. The **stretching** band at **3570 cm⁻¹** obviously decreased in intensity for the coatings sprayed at 80 mm and almost disappeared for the coatings sprayed at **160 mm**. As it was mentioned before, during plasma spraying, the HA powders were dehydroxylated and some of the OH in the crystalline HA was lost, so the HA **was** partly transformed into **OAp**,⁸ which became a solid solution in HA; **i.e.**, OHA at room temperature. Due to the similar structure between HA and **OAp**, or OHA, this difference can not be easily identified by XRD. So it can be concluded that the originally identified HA are actually OHA. The HA powders were subjected to more dehydroxylation at longer SOD; thus, the **3570 cm⁻¹** band **was** almost invisible for the **coatings** sprayed at 160 mm as shown in Fig. 3. It has been shown by XRD that the coatings sprayed at **160 mm** were much more amorphous than those sprayed at 80 mm, so the **FTIR results** also verified that the two characteristic OH bands of HA did not exist in the amorphous phase. Further investigations are needed to distinguish between **OAp** or OHA.

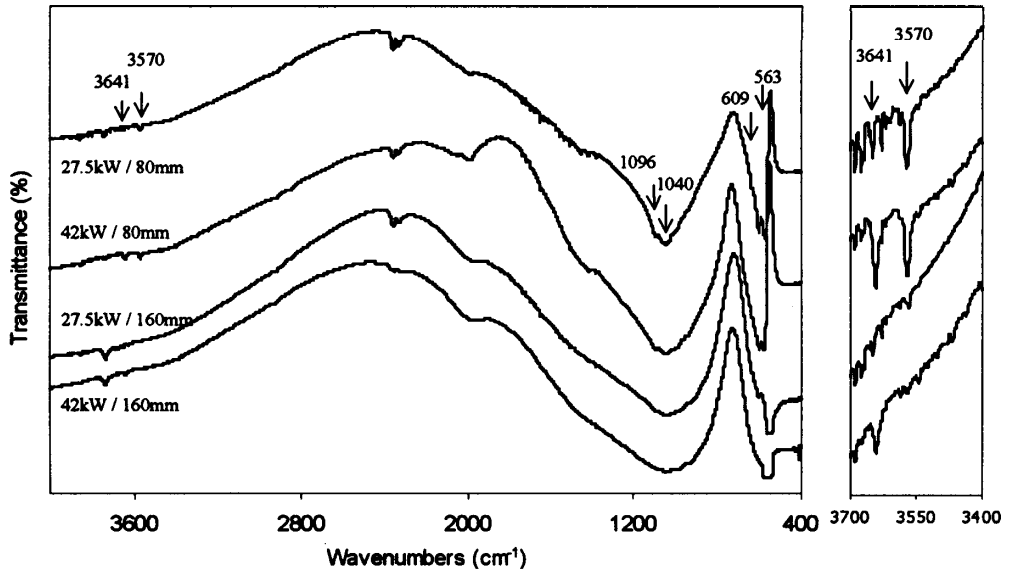
In addition to the above two OH bands, a new OH band appeared at **3641 cm⁻¹** in the spectra of HA coatings, which is not from the HA structure, but related to the **surface Ca(OH)₂ phase**.¹⁷ This band is very obvious in the spectra of the coatings sprayed at **42 kW**, but not obvious in coatings prepared at **27.5 kW**. This is consistent with the XRD results since coatings sprayed at **42 kW** demonstrate higher decomposition and **CaO** contents.

The **crystallinity** of the HA coatings can also be quantitatively determined using **FTIR** according to **Termine** and **Posner**.¹⁸ They found that the **FTIR** spectra of HA exhibited a gradual

splitting of the ν_4 band at 600 cm^{-1} from a broad singlet for **ACP** to a well-defined doublet for the fully crystalline HA. The splitting function (SF) was calculated as the ratio of the splitting area (formed by **connecting** the two minimum transmission points on the band) to the area limits of the band (formed by drawing a base line at the high transmission ends of the absorption band). Thus, the SF is zero for a complete **ACP** where a single broad peak exists and increased with the crystallinity. This method was appropriate for the two coatings sprayed at **80 mm**, which are relatively crystalline. But for the two rather amorphous coatings, the area limits were not easy to determine due to the shape of the band as shown in Fig. 3. On the other hand, as mentioned before, the splitting of the ν_3 band at 1040 cm^{-1} and 1096 cm^{-1} also increased with the crystallinity of HA coatings.



(a) HA powders

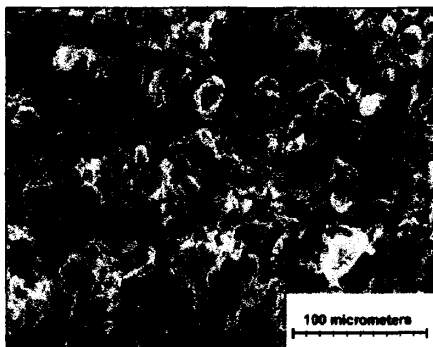


(b) HA coatings

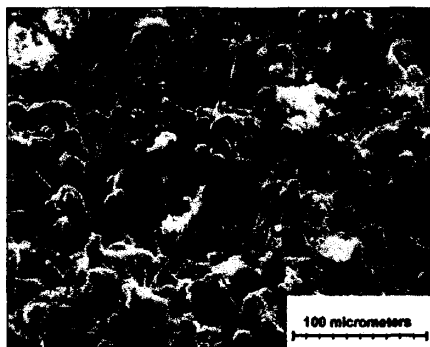
Figure 3. FTIR spectra of HA powders (a) and plasma sprayed HA coatings (b)

Surface Morphology and Roughness

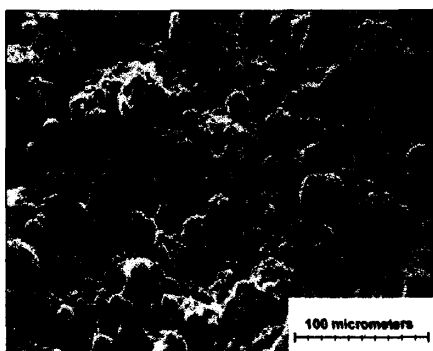
The surface morphologies of the HA coatings are shown in Fig. 4. The morphology of the coating sprayed at **27.5 kW** and 80 mm (Fig. 4a) was dominated by **unmelted** and partially melted particles over a small amount of flattened splats. These particles were quite large with a partially melted skin or have been crushed into fine particles which spread on the **splat**. This result is consistent with the XRD result since this coating exhibits the highest crystallinity. Even at the same power (**27.5 kW**), the coating morphology changed significantly when the SOD increased to **160 mm**, as shown in Fig. 4b. Despite some **unmelted** fine particles, the morphology was mainly composed of glassy phases including flattened splats, accumulated splats and spheroidized particles. No large particles existed in this morphology. Such morphological features agree with the explanation for the XRD results presented previously; *i.e.*, some of the **unmelted** larger particles were blown away before they impacted on the substrate at longer SOD. In addition, at longer SOD, the particle velocity decreased, so even if **some** particles were wholly melted, they were **transformed to spheroidized** particles or accumulated splats instead of flattened splats. The morphologies of the coatings sprayed at **42 kW** (Fig. 4c and 4d) showed that the particles were much better melted, which also mirrored the XRD results. The coating sprayed at 80 mm (Fig. 4c) mainly consisted of flattened and accumulated splats as well as **some** spheroidized and partially melted particles. On the other hand, for the coatings sprayed at **160 mm** (Fig. 4d), almost all **powders** were melted and the main characteristics were glassy flattened and accumulated splats as well as some spheroidized particles.



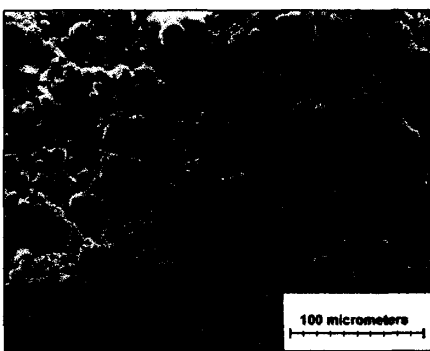
(a) 27.5 kW / 80 mm



(b) 27.5 kW / 160 mm



(c) 42 kW / 80mm



(d) 42 kW / 160 mm

Figure 4. **Surface** morphologies of plasma sprayed HA coatings

The surface roughness of the HA coatings, Fig. 5, reflects the irregular morphology of the coating surface. The coating sprayed at 80 mm generally resulted in rougher surface with the coexistence of several surface characteristics (e.g., partially melted particles, **accumulated splats**, flattened splats and **spheriodized** particles) while the longer SOD lead to a lower roughness. The coating sprayed at 27.5 kW and 80 mm also exhibits a low **surface** roughness since its morphology is dominated by the **unmelted** powders.

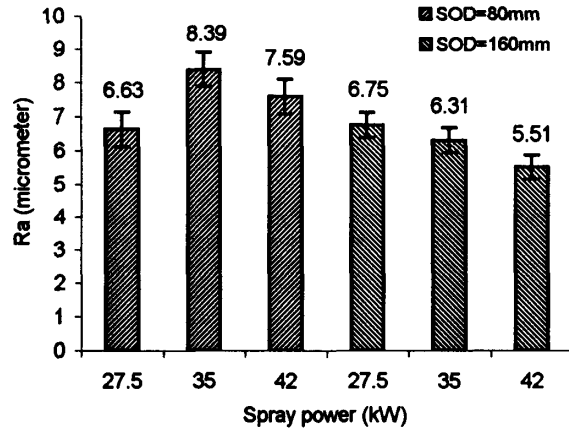


Figure 5. Surface roughness of plasma sprayed HA coatings

CONCLUSIONS

Plasma sprayed HA coating surfaces were characterized using XRD, FTIR, SEM and profilometry and the following conclusions made:

- (1) The HA **coatings** have different composition and structure **from** those of the feedstock HA powders. XRD revealed the presence of crystalline HA, **ACP** and some crystalline impurities including α -TCP, **β -TCP**, **TTCP** and **CaO**. FTIR reflected the changes of both OH and PO_4^{3-} bands after spraying and showed that the HA phase identified by XRD was actually OHA.
- (2) The phase composition of HA coatings varied with respect to the spray parameters. The crystallinity decreased with increasing spray power and SOD, the TCP, TTCP and CaO contents increased with the spray power while the CaO contents were **significant** at both higher power and longer SOD. The original OH band characteristic of HA at 3570 cm^{-1} decreased in intensity for coatings sprayed at 80 mm while it almost disappeared for coatings sprayed at 160 mm. **All** these effects were related to the melting, dehydroxylation, decomposition, cooling rate and deposition efficiency in the plasma spray process.
- (3) The surface morphology of the coating sprayed at higher power and longer SOD revealed much better particle melting, and the surface roughness reflected the irregular morphology of the surface, which were all consistent with the phase composition analysis.

NOMENCLATURE

ACP:	Amorphous calcium phosphate	APS:	Atmospheric plasma spray
FTIR:	Fourier transform infrared spectroscopy	HA:	Hydroxyapatite
OAp:	Oxyapatite	OHA:	Oxyhydroxyapatite
SEM:	Scanning electron microscopy	SOD:	Stand-off distance
TCP:	Tricalcium phosphate	TTCP:	Tetracalcium phosphate
XRD:	X-ray diffraction		

ACKNOWLEDGMENTS

This work is supported in part under **NSF-MRSEC DMR** grant number 9632570. The authors would like to thank Matthew R. Gold, **Christienne E. Mancini** and **Lionel Keene** for their help.

REFERENCES

- ¹Y.c. **Tsui**, C. Doyle, T.W. Clyne, *Biomaterials*, "Plasma sprayed hydroxyapatite coatings on titanium substrates Part I: Mechanical properties and residual stress levels," 19,2015-29 (1998)
- ²**C.C. Bemdt**, G.N. **Haddad**, A.J.D. Farmer and K.A. Gross, "Thermal spraying for **bioceramic** applications," *Mater. Forum*, 14,161-73 (1990)
- ³**P. Ducheyne**, L.L. Hench, A. Kagan, M. Martens, A. **Burssens** and J.C. **Mulier**, "The effect of hydroxyapatite impregnation on skeletal bonding of porous coated implants," *J. Biomed. Mater. Res.* 14,225-37 (1980)
- ⁴**P. Ducheyne** and K. **Healy**, "The effect of plasma sprayed calcium phosphate ceramic coatings on the metal ion release from porous titanium and cobalt chromium alloys," *J. Biomed. Mater. Res.* 2, 1137-63 (1988)
- ⁵**K.A. Gross** and C.C. Bemdt, "Optimization of spraying **parameters** for hydroxyapatite," in *Proc. 2nd Plasma-Technik Symposium*, 3, ed. S. **Blum-Sandmeier**, H. **Eschnauer**, and P. Huber, **Plasma-Technik AG**, Wohlen, Switzerland, 159-70 (1991)
- ⁶**M. Ogiso**, Y. **Yamashita** and T. **Matsumoto**, "Difference in **microstructural** characteristics of dense HA and HA coating," *J. of Biomed Mater Res.* 41,296-303 (1998)
- ⁷**L. Sun**, C.C. **Bemdt**, **R Lima**, A. **Kucuk** and **K.A. Khor**, "Effects of spraying parameters on phase formation and distribution in plasma sprayed hydroxyapatite coatings," accepted by the International Thermal Spray Conference - **ITSC2000**, May 8-11, 2000, Montreal, **Canada**. Ed. C.C. Bemdt, ASM Int., Materials Park, OH (2000)
- ⁸**S.R. Radin** and P. Ducheyne, "Plasma spraying induced changes of calcium phosphate ceramic characteristics and the effect on *in vitro* stability," *J. Mater. Sci. Mater. Med.* 3, 3342 (1992)
- ⁹**J.C. Trombe** and G. Montel, "Some features of the incorporation of oxygen in different **oxydation** states in apatite lattice," *J. Inorg. Nucl. Chem.* 40, 15-21 (1978).
- ¹⁰**R.Z. LeGeros**, "Biodegradation and **bioresorption** of calcium phosphate ceramics," *Clin. Mater.*, 14, 65-68 (1993)
- ¹¹**D.R. Lide**, editor. **Handbook of Chemistry and Physics. 71st CRC:Boca Raton; 1990**, p. 8-39
- ¹²**K. Hyakuna**, T. **Yamamuro**, Y. Kotoura, M. **Oka**, T. **Nakamura**, T. Kitsugi, T. **Kokubo** and H. **Kushitani**, "Surface reactions of calcium phosphate ceramics to various solutions," *J. Biomed. Mater. Res.* 21,471-88 (1990)
- ¹³**Selected Powder Diffraction Data for Minerals**, 1st Ed. Joint **Committee** on Powder Diffraction Standard, JCPDS, Philadelphia, PA (1974)
- ¹⁴**R. McPherson** and N. Gane, "Structural characterization of plasma-sprayed hydroxylapatite coatings," *J. Mater. Sci. Mater. Med.*, 6,327-34 (1995)
- ¹⁵**S.R. Levitt**, *The Vibrational Spectroscopy And Normal Coordinate Analysis Of Geological Apatites*, Ph.D. thesis, Alfred University, Alfred, New York (1969)
- ¹⁶**E. Park**, R.A. **Condrate**, Sr. and D. Lee, "Infrared spectral investigation of plasma sprayed coated hydroxyapatite," *Materials Letters*, 36,3843 (1998)
- ¹⁷**A. Slosarczyk**, C. **Paluszkiwicz**, M. **Gawlicki** and Z. **Paszkiwicz**, "The FTIR spectroscopy and QXRD **studies** of calcium phosphate based materials produced **from** the powder precursors with different Ca/P ratios," *Ceramics International*, 23, 297-304 (1997)
- ¹⁸**J.D. Termine** and A.S. Posner, "Infra-red determination of the percentage of crystallinity in **apatitic** calcium phosphate," *Nature*, 211,268-70 (1966)